EFFECT OF HOT ISOSTATIC PRESSING ON THE MICROSTRUCTURAL EVOLUTION AND TENSILE PROPERTIES OF LASER POWDER BED FUSION-PROCESSED Co-BASED SUPERALLOY MAR-M-509A

[1]Kateřina SKOTNICOVÁ, [1]Tomáš ČEGAN, [1]Jan JUŘICA, [2]Marek PAGÁČ

[1] *Faculty of Materials Science and Technology, VSB – Technical University of Ostrava, Ostrava, Czech Republic, EU, katerina.skotnicova@vsb.cz*

[2] *Faculty of Mechanical Engineering, VSB – Technical University of Ostrava, Ostrava, Czech Republic, EU, marek.pagac@vsb.cz*

https://doi.org/10.37904/metal.2025.5150

Abstract

Superalloys based on Ni, Ni-Fe, and Co are among the most used metallic materials for high-temperature applications due to their excellent strength, creep and corrosion resistance. Co-based superalloys, in particular, offer superior corrosion resistance compared to Ni-based counterparts, making them ideal for long-lasting components subjected to moderate static or cyclic loads at elevated temperatures. However, their high hardness and strength pose significant challenges in machining, increasing production costs. To overcome these limitations, research has increasingly focused on additive manufacturing techniques that enable the fabrication of complex geometries with reduced material waste. This study investigates the feasibility of producing the Co-based superalloy Mar-M-509A using laser beam powder bed fusion (LB-PBF) followed by post-processing heat treatment. Components fabricated by laser powder bed fusion (LB-PBF) typically exhibit inherent internal porosity, microstructural anisotropy, and elevated residual stresses due to the rapid solidification and layer-wise nature of the process. These deficiencies necessitate the application of post-processing techniques, such as heat treatment or hot isostatic pressing (HIP), to enhance the microstructural integrity and mechanical performance of the material. This study examines the influence of various LB-PBF process parameters on the relative density of printed components and evaluates the effects of heat treatment and HIP on the microstructure and tensile properties. Heat treatment aimed at relieving internal stresses resulted in a yield strength of up to 980 MPa with an elongation of 6.5 %. In contrast, HIP treatment led to a reduction in yield strength to 730 MPa but significantly improved elongation to 9.9 %. The microstructural evolution induced by HIP and its impact on mechanical performance are analysed and discussed in detail.

Keywords: Powder bed fusion, heat treatment, hot isostatic pressing, tensile strength

1. INTRODUCTION

Additive manufacturing (AM) has drawn wide research attention around the world. Different from traditional manufacturing technologies, AM is a layer-by-layer approach [1]. Laser powder bed fusion (LB-PBF) is a type of metallic AM technique using a powder bed as the basic fabrication mode, in which the component is built by the powders with sizes of 15–50 μm using a high-energy laser beam. The LB-PBF process has several advantages as follows: (i) It is suitable for the fabrication of geometrically complex and free designs; (ii) it saves materials via powder recycling; (iii) it is highly precise and requires only a few or no post-processing steps [1,2]. However, this method also has certain shortcomings, primarily the frequent occurrence of internal porosity, which quantity can be modified by using appropriate printing parameters, but the occurrence of porosity cannot be completely eliminated [1-4]. Another drawback is the high internal stress in the products

caused by rapid solidification during printing and anisotropy of the microstructure and mechanical properties [1-5]. For the above reasons, it is always recommended to perform a heat treatment after printing that reduces internal stress and reduces anisotropy [6,7].

Superalloys are a unique class of high-strength alloys that have good resistance to oxidation and corrosion and excellent resistance to creep and rupture at elevated temperatures [7]. Co-based superalloys, for example, are less susceptible to hot-corrosion than Ni-based superalloys, which makes them a desirable material for static, long-lived parts that experience relatively low stresses at high temperatures [7,8]. However, their high hardness and strength pose significant challenges in machining, increasing production costs. Their preparation by the LB-PBF method is therefore very promising. Several publications [7-10] have already been published on the aforementioned Co superalloy prepared using LB-PBF, which demonstrate that using appropriate printing parameters, leads to products without significant porosity and with a fine microstructure typical of LB-PBF, anisotropy of the microstructure and relatively good mechanical properties. However, they focus on appropriate preparation parameters, build orientation and the influence of subsequent heat treatment [7-10]. This article deals with this alloy from a different perspective namely by effect of used printing parameters on porosity and effect of HIP processing on the elimination of porosity and mechanical properties. The use of faster printing parameters can reduce the overall cost of the product and for applications such as in the aerospace industry, HIP processing is usually required due to the increase in the service life of components due to the elimination of internal defects.

2. MATERIALS AND METHODS

Figure 1a presents the input powder used for the fabrication of all analysed samples. The powder, supplied by Oerlikon, exhibited a predominantly spherical morphology with particle sizes reaching up to 50 µm. The particle size distribution, determined using a MasterSizer 3000 analyser, revealed D10, D50, and D90 values of 19 µm, 32 µm, and 52 µm, respectively. The chemical composition of the powder (in wt%) was as follows: 55% Co, 24% Cr, 10% Ni, 7% W, 3.5% Ta, and 0.5% C.

Densification via laser-based powder bed fusion (LB-PBF) was carried out using two different machines: the Trumpf TruPrint 1000 and the Renishaw AM500. The experimental plan followed a Taguchi L16 orthogonal array design, supplemented by additional parameter sets employing higher laser power and the second printer model. All samples were fabricated as cylindrical rods with a diameter of 13 mm and a length of 80 mm, printed in a horizontal orientation as shown in **Figure 1b**. The specific processing parameters and printer type used for each sample set are detailed in **Table 1.**

(a) (b)

Figure 1 (a) SEM micrograph of input powder; (b) prepared rod samples in the building platform

Following fabrication, all samples underwent heat treatment (HT) in a dynamic argon atmosphere using a Xerion XVAC furnace. The process was conducted at 500 °C for 2 hours, including the build platform, with the aim of relieving residual stresses induced during the LB-PBF process. After HT, the samples were detached from the platform via electrical discharge machining (EDM) using a CHMER EDM system.

Subsequently, transverse and longitudinal sections were extracted from the cylindrical bars using EDM to enable metallographic characterization and pycnometric density measurements. Standard metallographic preparation procedures were employed, including grinding with SiC abrasive papers (grit sizes from 60 to 2000 grains/cm²), followed by polishing using Al_2O_3 suspensions with progressively decreasing particle sizes (from 1.0 µm to 0.3 µm).

Microstructural analysis was conducted using optical microscopy (OM) on an Olympus GX51 microscope and scanning electron microscopy (SEM) using a Quanta 450 FEG instrument equipped with an energy-dispersive X-ray spectroscopy (EDS) detector. Kalling's reagent was applied for etching to reveal the microstructural features. Sample density (ρ_{pyc}) was determined by helium pycnometry using an AccuPyc II 1340 gas pycnometer with an integrated analysis module. Closed porosity (P_{cl}) was calculated according to the equation:

$$P_{cl} = (1 - \rho_{pyc}/\rho_{teo}) \times 100 \quad (1)$$

where ρ_{teo} represents theoretical density of Mar-M-509A, taken as 8.86 g/cm³. For each sample, the final density value was derived from the average of 10 measurement cycles. In addition, porosity levels were evaluated by image analysis (P_{ia}) using ImageJ software. This method involved adjusting the brightness threshold to distinguish dark pores from the bright matrix. Porosity fractions were calculated automatically, based on digitalized OM images acquired at 100× magnification. Five distinct regions were analysed per sample, with locations distributed across the x-axis from edge to edge.

Samples from series 18 were further subjected to HIP at 1260 °C under a pressure of 190 MPa for 2 hours using an EPSI HIP system. To evaluate the effect of HIP on mechanical properties, tensile tests were performed on samples from series 17 (as-printed) and series 18 (HIP-treated). Tensile specimens, with dimensions of 8 mm thickness and 55 mm gauge length, were tested using a Zwick/Roell Z150 universal testing machine at a constant strain rate of 0.5 min^{-1}. The Vickers microhardness in transverse (HV_{mT}) and longitudinal (HV_{mL}) sections was measured on the FM-ARS900 device at a load of 200 g for 7 s.

Table 1 Processing parameters used for LB-PBF. Scanning strategies: CH – Chessboard, M – Meander, S – Stripes. Printing systems: T – Trumpf TruPrint 1000, AM – Renishaw AM500.

Sample	1	2	3	4	5	6	7	8	9
Laser power (W)	125	125	125	125	140	140	140	140	155
Scanning speed (mm/s)	460	710	960	1210	460	710	960	1210	460
Scan strategy	CH	CH	M	M	M	M	CH	CH	CH
Layer high (µm)	20	20	20	20	20	20	20	20	20
Hatch distance (µm)	110	110	110	110	110	110	110	110	110
Printer type	T	T	T	T	T	T	T	T	T
Preheating (°C)	-	-	-	-	-	-	-	-	-
Sample	**10**	**11**	**12**	**13**	**14**	**15**	**16**	**17**	**18**
Laser power (W)	155	155	155	170	170	170	170	330	330
Scanning speed (mm/s)	710	960	1210	460	710	960	1210	1000	1000
Scan strategy	CH	M	M	M	M	CH	CH	S	S
Layer high (µm)	20	20	20	20	20	20	20	60	60
Hatch distance (µm)	110	110	110	110	110	110	110	110	110
Printer type	T	T	T	T	T	T	T	AM	AM
Preheating (°C)	-	-	-	-	-	-	-	170	170

3. RESULTS AND DISCUSSION

Table 2 shows the resulting values of pycnometric density measurements and contents of closed porosity computed from density values and contents of porosity detected by image analysis. As can be seen in this table, the use of different parameters (see **Table 1**) does not cause significant differences in the porosity content. Although the use of a higher scanning speed, especially for prints prepared with lower laser powers (samples 4,8), shows higher porosity contents (which was revealed mainly by image analysis), the values are not very different, and the use of higher laser powers reduces the effect of the higher speed used. This Co superalloy therefore does not show a significant influence on the porosity content due to different printing parameters, as was determined, for example, for 316L steels in which the use of a scanning speed of 1200 mm/s led to the formation of lack of fusion porosity and its content was up to 19 % [11].

Table 2 Results of pycnometric density measurements and contents of closed porosity computed from density values and contents of porosity detected by image analysis

Sample	**1**	**2**	**3**	**4**	**5**	**6**	**7**	**8**	**9**
ρ_{pyc} (g/cm^3)	8.829	8.816	8.807	8.787	8.8294	8.822	8.802	8.788	8.829
P_{cl} (%)	0.35	0.50	0.59	0.83	0.35	0.43	0.66	0.81	0.35
P_{ia} (%)	0.06	0.05	0.18	0.21	0.07	0.08	0.14	0.19	0.11
Sample	**10**	**11**	**12**	**13**	**14**	**15**	**16**	**17**	**18**
ρ_{pyc} (g/cm^3)	8.824	8.814	8.811	8.832	8.824	8.816	8.802	8.829	8.829
P_{cl} (%)	0.41	0.52	0.55	0.32	0.40	0.50	0.65	0.35	0.35
P_{ia} (%)	0.04	0.08	0.05	0.05	0.01	0.02	0.13	0.06	0.08

Figure 2 presents optical microscopy images illustrating the porosity distribution in the prepared Co-based superalloy samples. As evident from the micrographs, the pores were predominantly smaller than 100 µm and randomly distributed throughout the material. In **Figure 2a** (sample 9), manufactured under relatively moderate energy input, the pores were uniformly dispersed and exhibited a consistently near-spherical morphology, indicative of gas entrapment during solidification. **Figure 2b** (sample 16), produced using parameters associated with high scanning speed, revealed larger and more irregular pores, likely resulting from melt pool instabilities and localized lack-of-fusion-induced porosity. In contrast, **Figure 2c** (sample 13), processed under more balanced conditions, showed a significantly reduced pore density, with only a few isolated, fine pores, suggesting effective densification and stable melt pool behaviour. These findings highlight the strong influence of process parameter combinations on pore formation mechanisms and support the coexistence of both gas-induced and keyhole-related porosity depending on the local energy distribution and melt pool dynamics [11,12].

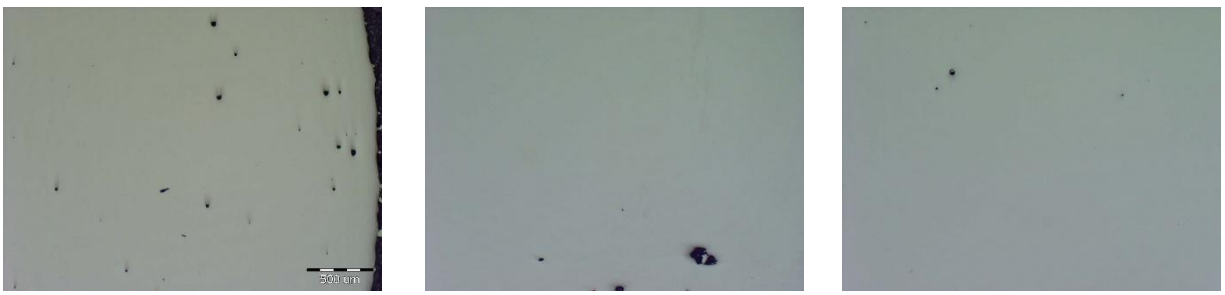

(a) (b) (c)

Figure 2 Microstructure of Co-based superalloy Mar-M-509A samples in the as-printed condition: (a) sample 9; (b) sample 16; (c) sample 13. All images correspond to transverse sections and were taken at the same magnification using optical microscopy (OM)

Figure 3a and **3b** documented the microstructure of the prepared samples, which exhibited typical scan track patterns in transverse sections and a “fish scale” morphology in longitudinal sections, corresponding to the layer-wise deposition and solidification inherent to the LB-PBF process. At higher magnifications (**Figures 3c-e**), the microstructure revealed a characteristic cellular morphology, with bright cellular boundaries enriched in tungsten (W) and tantalum (Ta), and darker cell interiors associated with depleted matrix regions. **Figure 3d** illustrated a distinct boundary between adjacent scan tracks, marked by variations in crystallographic orientation and cellular morphology, indicative of grain boundaries formed during rapid solidification.

The microstructure observed after LB-PBF followed by heat treatment at 500 °C for 2 hours exhibited pronounced anisotropy and morphological heterogeneity, both characteristic of LB-PBF-produced components. **Figure 3f** showed the microstructure after HIP processing. The cellular architecture was no longer visible, suggesting that the applied HIP temperature of 1260 °C for 2 hours was sufficient to dissolve the W- and Ta-rich cell walls. Bright regions observed in **Figure 3f** corresponded to carbides (Ta, W, Cr), up to 1 µm in size, which were relatively uniformly distributed throughout the matrix. These observations were consistent with the findings reported by Ferreri [9] following heat treatment at 1260 °C. HIP processing therefore resulted in a fully transformed microstructure and significantly reduced the porosity content, down to 0.02 % based on pycnometric measurements, and 0.01 % as determined by image analysis of metallographic cross-sections.

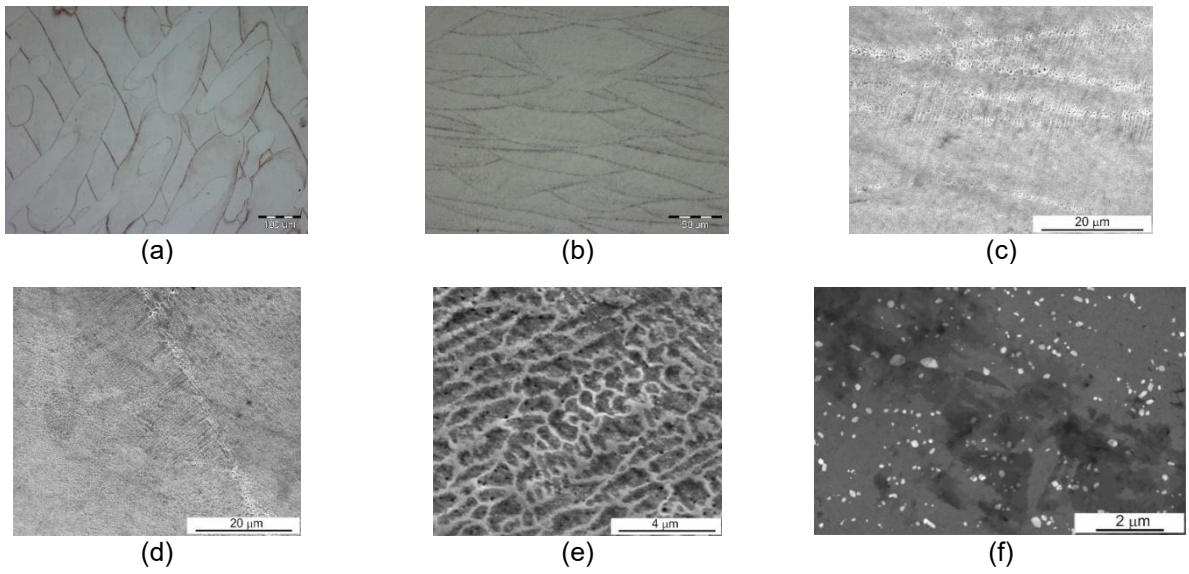

(a) (b) (c)

(d) (e) (f)

Figure 3 Microstructure of selected Co-based superalloy Mar-M-509A samples: (a) sample 1, transverse section, optical microscopy (OM); (b) sample 1, longitudinal section, OM; (c) sample 5, longitudinal section, scanning electron microscopy (SEM); (d) sample 10, transverse section, SEM; (e) sample 5, transverse section, SEM; (f) sample 18 after HIP treatment, longitudinal section, SEM

Figure 4 presents the engineering stress–strain curves obtained from tensile testing of specimens from series 17 (as-printed and heat-treated), labelled as Co_A, and from series 18 (after HIP), labelled as Co_B. The corresponding mechanical property values are summarized in **Table 3**. As evident that the application of HIP led to a reduction in average yield strength, accompanied by a notable increase in ductility, indicating improved resistance to crack propagation. The HIP treatment also resulted in a decrease in Vickers microhardness, observed in both transverse (T) and longitudinal (L) cross-sections (see **Table 3**). The observed reductions in yield strength and microhardness are likely associated with microstructural changes, particularly the elimination of the cellular substructure commonly formed during rapid solidification in LB-PBF.

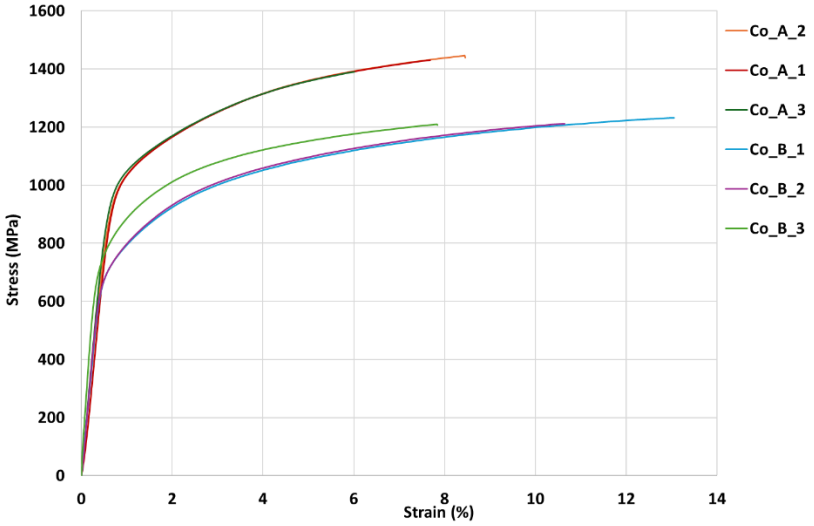

Figure 4 Strain-stress curves from tensile testing

Despite these decreases, both the HT-treated series 17 and HIP-treated series 18 exhibited significantly higher yield strength values compared to the cast alloy of identical chemical composition, which typically shows yield strengths below 600 MPa [7]. For comparison, Ghorbanpour [7] reported a yield strength of 690 MPa for LB-PBF fabricated MAR-M-509 in the horizontal build direction. Ferreri [9] reported even lower yield strengths for vertically printed (820 MPa) and heat-treated (690 MPa, 6 h at 1260 °C) samples, but observed higher ultimate tensile strengths of 1540 MPa and 1530 MPa, and elongations of 10 % and 22 %, respectively.

Table 3 Resulting mechanical property values of tensile testing and microhardness measurements

Sample	E (GPa)	$R_{p0.2}$ (MPa)	R_m (MPa)	A (%)	Z (%)	HV_{mT}	HV_{mL}
Co_A	173 ± 10	983 ± 20	1423 ± 29	6.55 ± 1,26	7.18 ± 0,69	483 ± 15	472 ± 15
Co_B	178 ± 9	732 ± 23	1218 ± 12	9.87 ± 2,50	7.78 ± 2,29	425 ± 8	437 ± 12

4. CONCLUSION

The Co-based superalloy Mar-M-509A was successfully processed via laser beam powder bed fusion (LB-PBF) using a wide range of processing parameters. The variations in laser power, scanning speed, and scanning strategy showed no statistically significant influence on the final porosity, which remained low across all samples (below 0.83 %). The as-built microstructure exhibited a fine cellular morphology, typical of rapid solidification in LB-PBF, and the samples demonstrated high mechanical performance, with a yield strength of 980 MPa and elongation to fracture of 6.5 %.

Post-processing via hot isostatic pressing (HIP) led to significant microstructural changes. The characteristic cellular substructure was no longer observed, and fine carbides appeared, uniformly distributed in the matrix. Although detailed phase analysis (e.g., XRD or TEM) is beyond the scope of this study, preliminary findings suggest that phase transformations likely occurred during HIP treatment, as evidenced by the disappearance of the cellular microstructure and the formation of uniformly distributed carbides. These transformations contributed to the observed decrease in yield strength and hardness, while simultaneously improving ductility.

These findings confirm that HIP not only enhances the structural integrity of LB-PBF-produced Mar-M-509A through effective densification but also promotes microstructural homogenization beneficial for increasing ductility. Despite a moderate reduction in strength, the overall balance of properties makes HIP a valuable post-processing step for components intended for demanding high-temperature applications where defect tolerance and reliability are essential.

ACKNOWLEDGEMENTS

This work was supported by the project TN02000018 "National Centre of Competence for Engineering" and by the project SP2025/080 "Development and implementation of a measuring device for sound absorption measurement of materials at low excitation frequencies".

REFERENCES

[1] FRAZIER, W.E. Metal additive manufacturing: a review. *Journal of Materials Engineering and Performance*. 2014, vol. 23, pp. 1917–1928. https://doi.org/10.1007/s11665-014-0958-z.

[2] DAR, J., PONSOT, A.G., JOLMA, C.J., LIN, D. A review on scan strategies in laser-based metal additive manufacturing, *Journal of Materials Research and Technology*. 2025, vol. 36, pp. 5425-5467, ISSN 2238-7854. https://doi.org/10.1016/j.jmrt.2025.04.068.

[3] MAHMOOD, M.A., ISHFAQ, K., OANE, M., LIOU, F. Porosity prediction in LPBF of AISI 316L stainless steel: Refined vol.tric energy density and FEM simulation approach, *Optics & Laser Technology*. 2025, vol. 188, p. 113015, ISSN 0030-3992. https://doi.org/10.1016/j.optlastec.2025.113015.

[4] GELATKO, M., HATALA, M., BOTKO, F., VANDŽURA, R., HAJNYŠ, J. Eddy current testing of artificial defects in 316L stainless steel samples made by additive manufacturing technology. *Materials*. 2022, vol. 15, p. 6783. https://doi.org/10.3390/ma15196783.

[5] HITZLER, L., HIRSCH, J., HEINE, B., MERKEL, M., HALL, W., ÖCHSNER, A. On the anisotropic mechanical properties of selective laser-melted stainless steel. *Materials*. 2017, vol. 10, no. 10, p. 1136. https://doi.org/10.3390/ma10101136.

[6] GELATKO, M., HATALA, M., BOTKO, F., VANDŽURA, R., HAJNYŠ, J., ŠAJGALIK, M., TOROK, J. Stress relieving heat treatment of 316L stainless steel made by additive manufacturing process. *Materials*. 2023, vol. 16, no. 19, p. 6461. https://doi.org/10.3390/ma16196461.

[7] GHORBANPOUR, S., BICKNELL, J., KNEZEVIC, M. Fatigue strength of additive manufactured Mar-M-509 superalloy. *Materials Science and Engineering: A*. 2022, vol. 840, p. 142913, ISSN 0921-5093. https://doi.org/10.1016/j.msea.2022.142913.

[8] CLOOTS, M., KUNZE, K., UGGOWITZER, P.J., WEGENER, K. Microstructural characteristics of the nickel-based alloy IN738LC and the cobalt-based alloy Mar-M509 produced by selective laser melting, *Materials Science and Engineering: A*. 2016, vol. 658, pp. 68-76, ISSN 0921-5093. https://doi.org/10.1016/j.msea.2016.01.058.

[9] FERRERI, N.C., GHORBANPOUR, S., BHOWMIK, S., LUSSIER, R., BICKNELL, J., PATTERSON, B.M., KNEZEVIC, M. Effects of build orientation and heat treatment on the evolution of microstructure and mechanical properties of alloy Mar-M-509 fabricated via laser powder bed fusion. *International Journal of Plasticity*. 2019, vol. 121, pp. 116-133, ISSN 0749-6419. https://doi.org/10.1016/j.ijplas.2019.06.002.

[10] GUO, CH., ZHOU, Y., XU, Z., LI, Y., LI, G., SHI, Z., SUN, J., HE, X., ZHU, Q. Macro Co-Al-W-based superalloy single-crystal fabrication using selective laser melting. *Scripta Materialia*. 2024, vol. 251, p. 116213, ISSN 1359-6462. https://doi.org/10.1016/j.ijplas.2019.06.002.

[11] CEGAN, T., PAGAC, M., JURICA, J., SKOTNICOVA, K., HAJNYS, J., HORSAK, L., SOUCEK, K., KRPEC, P. Effect of hot isostatic pressing on porosity and mechanical properties of 316L stainless steel prepared by the selective laser melting method. *Materials*. 2020, vol. 13, no. 19, p. 4377. https://doi.org/10.3390/ma13194377.

[12] BAYAT, M., THANKI, A., MOHANTY, S., WITVROUW, A., YANG, S., THORBORG, J., TIEDJE, N.S., HATTEL, H.H. Keyhole-induced porosities in Laser-based Powder Bed Fusion (L-PBF) of Ti6Al4V: High-fidelity modelling and experimental validation. *Additive Manufacturing*. 2019, vol. 30, p. 100835, ISSN 2214-8604. https://doi.org/10.1016/j.addma.2019.100835.